Quantized zero-bias conductance plateau in semiconductor-superconductor heterostructures without topological Majorana zero modes

Christopher Moore,[1] Chuanchang Zeng,[1] Tudor D. Stanescu,[2] and Sumanta Tewari[1]
[1]*Department of Physics and Astronomy, Clemson University, Clemson, South Carolina 29634, USA*
[2]*Department of Physics and Astronomy, West Virginia University, Morgantown, West Virginia 26506, USA*

(Received 21 May 2018; revised manuscript received 25 September 2018; published 19 October 2018)

Recent observations of robust zero-bias quantized conductance plateaus of height $2e^2/h$ in quantum dot-semiconductor-superconductor nanowire heterostructures have been interpreted as clear evidence for the presence of non-Abelian topologically protected Majorana zero modes (MZMs), since other sources of low-energy conductance are believed to be unable to produce such quantized plateaus. Based on extensive numerical calculations, we show that, in fact, quantized conductance plateaus of height $2e^2/h$ can also arise as a result of *partially separated* Andreev bound states (ps-ABSs), in which the component Majorana bound states are somewhat shifted in space without being topological MZMs. As ps-ABSs can form rather generically in the topologically trivial phase, even in the absence of disorder, our results conclusively establish that the observation of quantized conductance plateaus of height $2e^2/h$ *does not* represent sufficient evidence for the existence of topologically protected MZMs localized at the opposite ends of a wire.

DOI: 10.1103/PhysRevB.98.155314

I. INTRODUCTION

Semiconductor nanowires with proximity-induced superconductivity and strong Rashba spin-orbit coupling, which are predicted theoretically [1–7] to support a pair of midgap non-Abelian Majorana zero modes (MZMs) at the opposite ends of a wire [8–12], have become the leading candidate for the realization of topological quantum computation (TQC) [9,10] due to the tremendous experimental progress realized in the past few years [13–24]. The most recent important development of far-reaching consequence to TQC has been the observation of quantized zero-bias conductance plateaus in local charge tunneling experiments [24], with the theoretically predicted height ($2e^2/h$) required by topological MZMs [25–28]. While previous theoretical work on proximitized semiconducting nanowires has shown the formation of zero-bias conductance peaks (ZBCPs) even in the absence of MZMs due to disorder [29–34], nonuniform system parameters [35–44], weak antilocalization [45], and coupling to a quantum dot [46,47], these peaks of non-Majorana origin *do not* result in a $2e^2/h$-quantized conductance plateau whose height remains constant against variations of the control parameters (e.g., Zeeman field, tunnel barrier height). Note that a quantized conductance plateau does not simply mean the presence of a robust zero-bias conductance peak (of arbitrary height) that sticks at zero energy as a function of the magnetic field or the realization of a quantized zero-bias peak of height $2e^2/h$ at some specific values of the control parameters but rather the persistence of a zero-bias peak with a constant quantized height of $2e^2/h$ over a finite range of control parameters such as the magnetic field and the tunnel coupling. This type of feature was so far believed to be associated with the presence of (topological) Majorana zero modes. Consequently, in the recent experiments [24] the quantized peaks of height $2e^2/h$ and the persistence of the plateaus against the variation of the control parameters have been used as a key evidence for the presence of topologically protected MZMs localized at the opposite ends of the experimental system. Here, we demonstrate that the quantized conductance plateaus can also have non-Majorana origins, emerging in the topologically trivial regime.

In this paper, we perform detailed numerical calculations of the experimental system [24], which is a quantum dot–semiconductor-superconductor (QD-SM-SC) nanowire heterostructure, and show that quantized conductance plateaus of height $2e^2/h$, which are robust over a large range of Zeeman fields and tunnel barrier potentials, are also possible due to the presence of low-energy Andreev bound states (ABSs) whose component Majorana bound states (MBSs) are somewhat shifted in space: the so-called partially separated ABSs (ps-ABS) introduced in Ref. [48]. The ps-ABSs, on the other hand, are topologically trivial and cannot be used in TQC because the separation of the component MBSs, which are localized on the *same* side of the wire, cannot be controlled externally [48].

Essentially, when coupling locally to a ps-ABS one couples strongly to only one of the constituent MBSs [see Fig. 1(i)], while the other remains "invisible." We thus arrive at the important result, relevant to the remarkable set of recent experiments [24] and all other tunneling conductance measurements preceding it [13–15,17–23], that the observation of quantized conductance plateaus in local charge tunneling experiments, even if of the theoretically predicted height $2e^2/h$, *cannot* be taken as the clinching evidence for the presence of non-Abelian MZMs, distinguished from other "non-Majorana" sources such as robust low-energy ABSs, as claimed in the experiments [24].

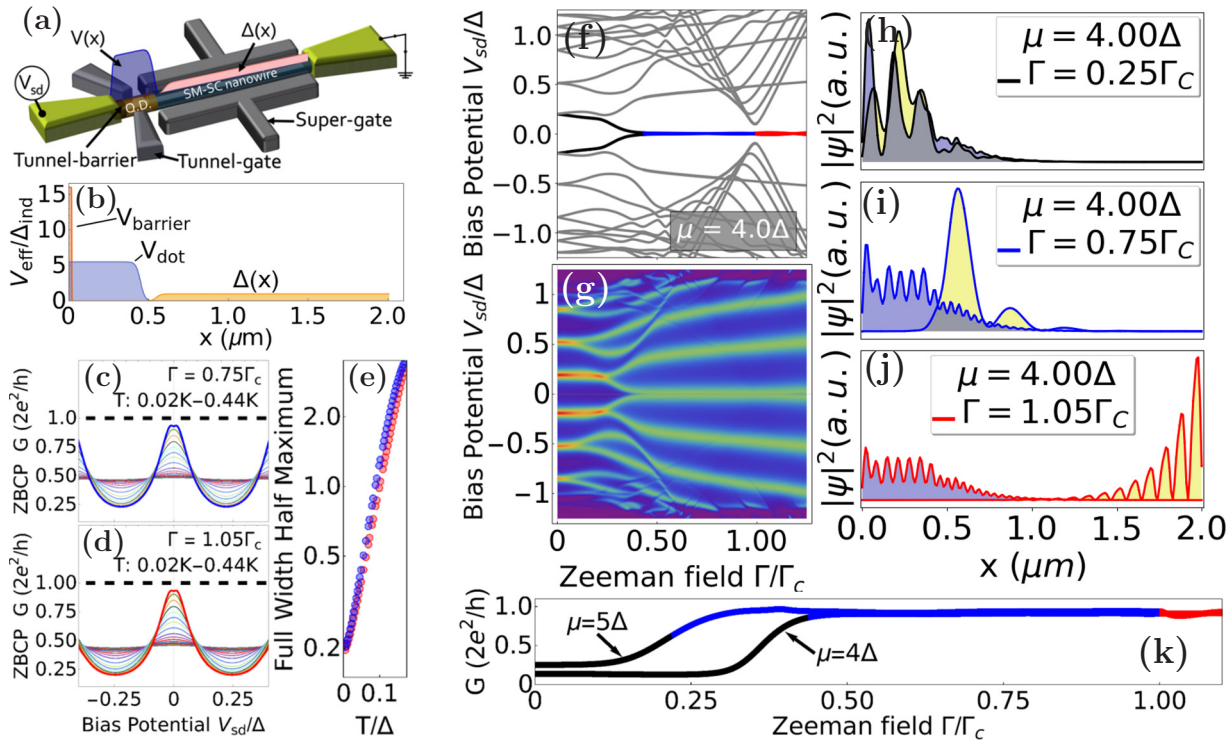

FIG. 1. (a) Proximitized nanowire junction in which a portion of the semiconductor wire (SM) is not covered by the superconductor (SC), represented by a quantum dot (QD). (b) Quantum dot potential $V(x) = V_{\text{barrier}} + V_{\text{dot}}$ as described by Eq. (2) may form within the QD due to a combination of tunnel coupling to the metallic lead (V_{barrier}) as well as application of the tunnel gate potentials (V_{dot}). Parameters used here were barrier potential height $Z = 16\Delta$ and width $x_t = 0.02\,\mu$m, and a quantum dot of width $x_0 \sim 0.5\,\mu$m with a potential height $V \sim 5.5\Delta$ which varies over a length scale of $\sigma_V \sim 27.5$ nm. Induced pairing $\Delta(x)$ described by Eq. (3) is present within the proximitized region of the wire. Here we used $\Delta_{\text{ind}} \sim 0.25$ meV, which varies over a length scale of $\sigma_\Delta \sim 27.5$ nm. Robustness of the zero bias peaks to different values of the barrier and dot potentials is shown in Fig. 2. [(c), (d)] Vertical line cuts from the differential conductance spectra shown in panel (g) showing a ZBCP quantized to $2e^2/h$ due to the presence of a ps-ABS (blue, Zeeman field $\Gamma < \Gamma_c$ with Γ_c being the critical field) and a MZM (red, $\Gamma > \Gamma_c$). Temperature dependence of ZBCP from 20 to 440 mK in steps of 20 mK shows gradual decrease of the peak height. (e) Full width at half maximum (FWHM) as a function of temperature T for ps-ABS (blue) and MZM (red) of curves taken from panels (c) and (d). (f) Low-energy spectra as a function of Zeeman field for a nanowire with the potential profile pictured in panel (b). The Zeeman field $\Gamma > \Gamma_c$ region is marked by the red zero-energy mode (MZM), while the blue zero mode marks the region supporting ps-ABSs. (g) Differential conductance spectra as a function of Zeeman field corresponding to energy spectra in panel (f). [(h)–(j)] Profiles of lowest energy mode wave functions: (h) A standard ABS consisting of a pair of overlapping MBSs, (i) a ps-ABS consisting of two overlapping MBSs whose separation is on the order of the Majorana decay length ζ, and (j) a pair of non-Abelian MZMs localized at opposite ends of the wire. (k) Zero-bias line cuts from conductance spectra showing $2e^2/h$-quantized conductance plateaus against variation of the Zeeman field for two representative values of the chemical potential due to the presence of a ps-ABS (blue) and MZM (red).

We interpret the results of this study within a framework based on two observations: (i) MZMs and ps-ABSs can be described theoretically using the same modeling of the hybrid structure. However, in the low-Zeeman-field regime, the ps-ABSs are significantly more common, because the parameter region corresponding to inhomogeneous systems that support ps-ABSs is much larger than the parameter region associated with nearly homogeneous systems that host MZMs. (ii) The goal of this study is *not* to identify the nature of the low-energy states responsible for the signatures observed experimentally (much less to demonstrate that these states are ps-ABSs). Given the fundamental uncertainty regarding key parameters of the hybrid systems used in experiments, such as, e.g., work function differences and couplings across the SM-SC interface, any attempt to solve these problems purely theoretically would be futile. The answer has to come from experiment. Here, we only show that the signature produced by a ps-ABS in a local tunneling measurement is indistinguishable from the corresponding signature of a MZM, *even if we test the robustness of this signature by varying the control parameters*.

II. SM-SC HETEROSTRUCTURE COUPLED TO A QUANTUM DOT

We consider a semiconductor (SM) nanowire with strong spin-orbit coupling, proximity coupled to a superconductor (SC) in the presence of an applied magnetic field. A portion of the SM wire is not covered by the SC, which may be thought of as a quantum dot [46–48]; see Fig. 1(a). The Bogoliubov–de Gennes (BdG) Hamiltonian for such a one-dimensional QD-SM-SC heterostructure can be written as

$$\tilde{H} = \left[-\frac{1}{2}\partial_{\tilde{x}}^2 - i\,\partial_{\tilde{x}}\sigma_y - \tilde{\mu} + V(\tilde{x})\right]\tau_z + \Gamma\sigma_x + \Delta(\tilde{x})\tau_x \quad (1)$$

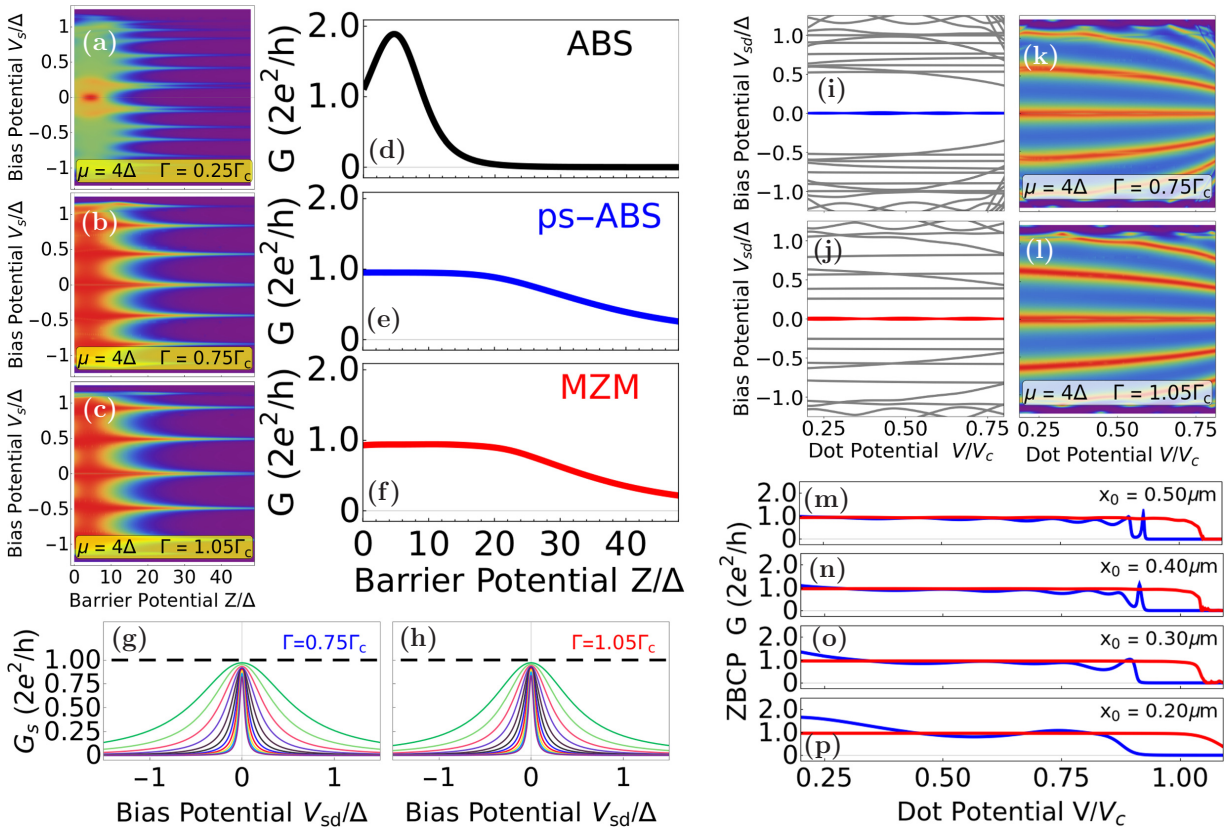

FIG. 2. [(a)–(c)] Differential conductance as a function of barrier height Z and bias potential associated with a standard ABS ($\Gamma = .25\Gamma_c$) (a), a ps-ABS ($\Gamma = .75\Gamma_c$) (b), and a pair of MZMs ($\Gamma = 1.05\Gamma_c$) (c). [(d)–(f)] Zero-bias line cuts for panels (a)–(c) showing the MZMs and ps-ABSs forming nearly identical profiles which plateau at $2e^2/h$ for a wide range of barrier heights. The standard ABS peak height (d) may take any value between 0 and $4e^2/h$ and quickly goes to 0 with increased barrier height. [(g), (h)] Vertical line cuts from panels (b) and (c) showing ZBCPs quantized at $2e^2/h$ over a large range of barrier potential heights Z for both ps-ABS and MZM. [(i), (j)] Low-energy spectra as a function of quantum dot potential height V associated with potential profile in Fig. 1(b) for ps-ABS (blue, $\Gamma < \Gamma_c$) and MZM (red, $\Gamma > \Gamma_c$). Here and in the following plots, $V_c = 2\mu$ is taken as the reference dot potential, while the dot potential V is varied between $.25V_c = 2\Delta$ and $V_c = 2\mu = 8\Delta$. [(k), (l)] Plots of differential conductance as a function of dot potential height V and bias potential for values consistent with energy spectra shown in panels (i) and (j). [(m), (p)] Horizontal zero-bias line cuts with panel (m) corresponding to panels (k)–(l) and panels (n)–(p) corresponding to identical systems with decreased QD lengths x_0, given in plots. The formation of a $2e^2/h$-quantized plateau can be seen for both ps-ABSs (blue) and MZMs (red) as a function of quantum dot potential and persists for a wide range of QD lengths x_0. As the length of the QD x_0 is decreased, the overlap between the constituent MBSs increases, and as a result the zero-bias conductance plateau associated with the ps-ABS (blue) becomes less robust to changes in the dot potential V.

with $\tilde{x} = m^*\alpha x$ and $\tilde{H} = (H/m^*\alpha^2)$. Here σ_i and τ_j are the Pauli matrices operating in spin and particle-hole spaces, respectively, Γ is the Zeeman field, and μ is the chemical potential. Parameters used were an effective mass $m^\star \approx 0.03m_0$ (m_0 being the electron mass) and a Rashba coefficient of $\alpha =$ 400 meV Å, consistent with the experiments. All calculations were done at a temperature $T \approx 20$ mK unless otherwise noted. Here $V(\tilde{x}) = V_{\text{barier}} + V_{\text{dot}}$, in which V_{barrier} represents the potential which arises due to tunnel coupling between the normal lead and the SM wire, and V_{dot} which is due to the tunnel gates shown in Fig. 1(b). The potential V_{dot} used throughout this paper is of the form

$$V_{\text{dot}} = \frac{V}{2}\left[1 - \tanh\left(\frac{\tilde{x} - x_0}{\sigma_V}\right)\right] \tag{2}$$

in which V is the height of the gate potential V_{dot} within the QD, x_0 is the length of the QD, and σ_V is the length scale over which V varies. The barrier potential V_{barrier} is taken as a sharp potential of height Z and width x_t, as shown in Fig. 1(b). The induced superconducting pair potential is

$$\Delta(\tilde{x}) = \frac{\Delta}{2}\left[1 + \tanh\left(\frac{\tilde{x} - x_0 + \delta_x}{\sigma_\Delta}\right)\right], \tag{3}$$

where Δ is the height of the pairing potential, δ_x is a parameter that controls the extension of the pairing potential in the QD region due to the proximity effect, and σ_Δ is the length scale over which Δ varies. In Fig. 1, we take $V = 5.5\Delta$, $\sigma_V = \sigma_\Delta = 25$ nm, $x_0 = 0.5\,\mu$m, $Z = 16\Delta$, $x_t = 0.02\,\mu$m, $\Delta = 0.25$ meV, and $\delta_x = 4\sigma_\Delta$.

The low-energy spectrum is obtained by numerically diagonalizing the BdG Hamiltonian corresponding to the nanowire. The robustness of the ZBCP is shown for different values of the barrier and dot potentials in Fig. 2. Values for the differential conductance G were found by discretizing the

Hamiltonian in Eq. (1) as follows:

$$\hat{H} = \sum_i (\psi_i^\dagger \{[2t - \mu + V(i)]\tau_z + \Gamma\sigma_x + \Delta(i)\tau_x\}\psi_i + [\psi_{i+a}^\dagger(-t\tau_z + i\alpha\sigma_y\tau_x)\psi_i + \text{H.c.}]) \quad (4)$$

written in the Nambu basis with $\psi_i = (c_{\uparrow i}, c_{\downarrow i}, c_{\uparrow i}^\dagger, c_{\downarrow i}^\dagger)$ in which i represents the lattice site and $t = 38\Delta$ is the hopping matrix element used throughout the calculations. The zero-temperature differential conductance

$$G_0(V) = \frac{e^2}{h}(N - R_{ee} + R_{he}), \quad (5)$$

was found using the S-matrix method [49]. Here N is the number of electron channels in the lead, R_{ee} is the total probability of normal reflection, and R_{eh} is the total probability of Andreev reflection for an electron in the lead. Finite temperature is represented by broadening the zero-temperature conductance through a convolution with the derivative of the Fermi function in the usual manner, $G(V,T) = -\int d\epsilon G_0(\epsilon) f_T'(\epsilon - V)$.

To analyze the low-energy ABSs, we represent the BdG eigenstates $\phi_{\pm\varepsilon}(i)$ of Eq. (4) as a pair of overlapping MBSs, $\chi_A(i) = \frac{1}{\sqrt{2}}[\phi_\varepsilon(i) + \phi_{-\varepsilon}(i)]$, and $\chi_B(i) = \frac{i}{\sqrt{2}}[\phi_\varepsilon(i) - \phi_{-\varepsilon}(i)]$. Using this formalism, a standard ABS is defined as a superposition of constituent MBSs that are sitting directly on top of one another [Fig. 1(h)], a ps-ABS as a superposition of constituent MBSs that are separated on the order of the Majorana decay length ζ [Fig. 1(i)], while topological MZMs correspond to constituent MBSs separated by the length of the wire [Fig. 1(j)]. From the wave function profiles, it is straightforward to see that if a ps-ABS is present in the quantum dot region, as in Fig. 1(i), a tunnel probe placed on the left-hand side of the wire will predominantly couple to a single MBS (purple), making it indistinguishable from a MZM, as in Fig. 1(j). Note that in a finite wire the bulk gap does not completely close and thus a ps-ABS can be continuously connected to a pair of non-Abelian MZMs. By contrast, in an infinite (or long) wire, in which the bulk gap closes signaling a TQPT, the ps-ABS and MZMs are separated by a quantum phase transition and only the pair of MZMs for $\Gamma > \Gamma_c$ are topologically nontrivial. Moreover, ps-ABSs cannot be used in TQC, because the separation between the component MBSs in a ps-ABS cannot be controlled independently.

III. RESULTS

In Fig. 1(f), we show the low-energy spectrum of the QD-SM-SC structure as a function of the applied Zeeman field. A pair of robust zero modes emerge in this plot (blue) well before the bulk band gap has a minimum signaling the TQPT. We associate these modes with ps-ABSs, while the zero-energy modes beyond the bulk gap closing (red) are topological MZMs. The corresponding plot of the differential conductance as a function of Zeeman field [Fig. 1(g)] shows a robust ZBCP in the topologically trivial regime indistinguishable from the ZBCP in the topological regime. Furthermore, Figs. 1(c)–1(e) show an exponential dependence of the ZBCP height and width on the temperature for both MZMs and ps-ABSs. These robust ZBCPs form $2e^2/h$-quantized conductance plateaus both in the topologically trivial and nontrivial regimes [Fig. 1(k)], similar to those observed in the experiments [24].

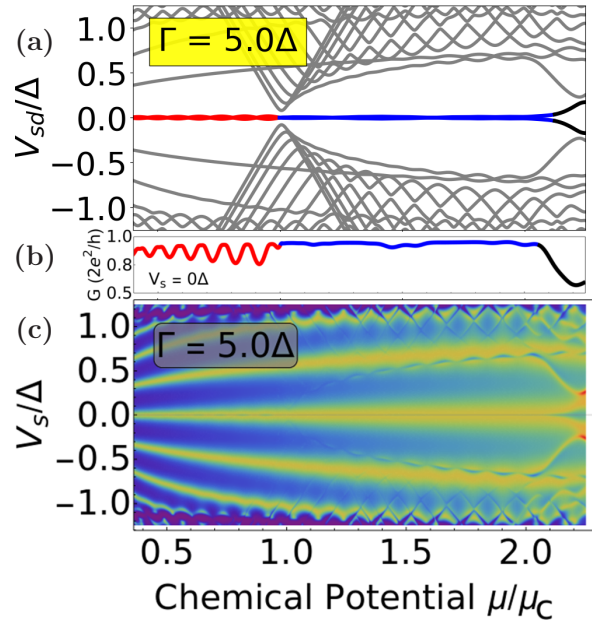

FIG. 3. (a) Low-energy spectra as a function of chemical potential. The red line signifies the topological region supporting MZMs, and the blue line shows a nontopological region supporting ps-ABSs which stick to zero energy for a wide range of chemical potential. (b) Zero-bias line cut taken from panel (c) showing a robust $2e^2/h$ quantized conductance plateau forming in the topologically trivial regime due to the presence of a ps-ABS. (c) Differential conductance spectrum as a function of chemical potential for parameter values consistent with Fig. 1.

Next, in Figs. 2(a)–2(f), we plot the differential conductance as a function of bias potential and barrier potential (Z). These results show that while the ZBCP height due to a standard ABS may take any value ($0 - 4e^2/h$) and quickly drops to zero upon increasing the barrier potential [Fig. 2(d)], the behavior of the ZBCPs induced by ps-ABSs and MZMs is nearly the same. Indeed, upon varying the barrier height, both the ps-ABS and the MZM induce (practically indistinguishable) quantized zero-bias conductance plateaus of height $2e^2/h$ [Figs. 2(e) and 2(f)]. The low-energy spectrum as a function of the quantum dot potential V corresponding to the potential profile shown in Fig. 1(b) is shown in Fig. 2(i) for a ps-ABS (blue, $\Gamma < \Gamma_c$) and in Fig. 2(j) for a MZM (red, $\Gamma > \Gamma_c$). The corresponding dependence of the differential conductance shown in Figs. 2(k) and 2(l), respectively, has similar (practically indistinguishable) features. Finally, the ps-ABS and the MZM have nearly identical $2e^2/h$-quantized conductance peaks that are robust against variations of the dot potential, as shown in Fig. 2(m).The dependence of the low-energy spectrum on the chemical potential, which experimentally can be controlled by changing the supergate potential, is shown in Fig. 3(a). A robust zero-energy mode emerges in the trivial regime (blue) due to a ps-ABS,

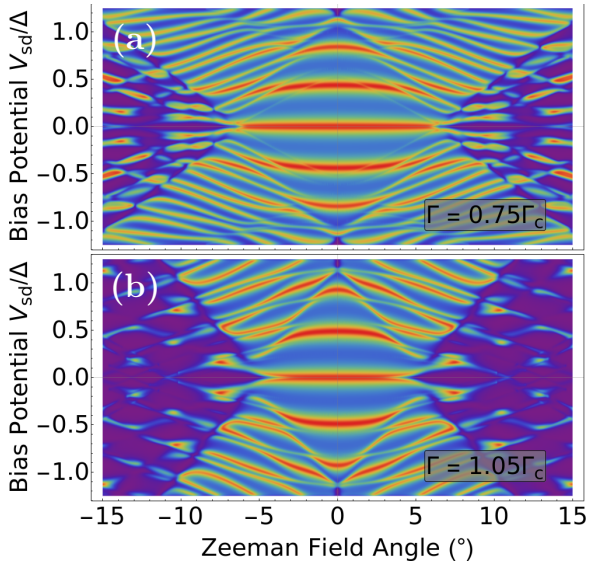

FIG. 4. Differential conductance as a function of the in plane angle of the Zeeman field for the ps-ABS (a) and the MZM (b) shown in Figs. 1(i) and 1(j). A ZBCP appears for a small angle in which the Zeeman field is almost aligned with the wire. As the angle between the wire and the direction of the Zeeman field is increased, the ZBCP is destroyed in both cases due to splitting.

well before the topologically nontrivial regime (red). This results in a robust $2e^2/h$-quantized conductance plateau as function of the chemical potential [Figs. 3(b) and 3(c)]. As in Ref. [24], the quantized ZBCP exhibits some oscillatory behavior due to peak splitting, with the ZBCP returning to the $2e^2/h$-quantized value but never exceeding it. Finally, SM-SC nanowires require a magnetic field oriented along the wire in order to support topological MZMs [1–7]. Reorientating the magnetic field toward the direction of the spin-orbit field should rapidly destroy the MZM-induced ZBCP [21]. The dependence of the differential conductance on the direction of the magnetic field is shown in Fig. 4 for both a trivial ps-ABS (a) and a MZM (b). In both cases, the ZBCP is only present for small values of the angle ϕ, for which the magnetic field is almost aligned with the direction of the wire.

IV. SUMMARY AND CONCLUSION

In summary, based on extensive numerical calculations, we show that quantized zero-bias conductance peaks, whose height remains constant at $2e^2/h$ as a function of varying system parameters such as Zeeman field, tunnel barrier height, dot potential, etc. (the so-called quantized conductance plateaus) [24], can arise as a result of partially separated Andreev bound states, in which the component Majorana bound states are somewhat shifted in space without being topological MZMs. As partially separated Andreev bound states can form generically in the topologically trivial phase, as illustrated in this paper with a steplike potential in the quantum dot region which can be induced by tunnel gates, we conclude that the recent experimental observations showing quantized conductance plateaus of height $2e^2/h$ as a function of various control parameters cannot represent definitive evidence for the presence of MZMs. We emphasize that a more "realistic" modeling of the experimental system (which would face major challenges, considering our limited knowledge of key microscopic parameters that characterize the hybrid systems studied experimentally) is not expected to modify this conclusion. Essentially, when coupling locally to the end of the quantum dot, which may harbor a ps-ABS, one couples much stronger to one of the constituent MBSs than to the other because of the partial separation between the pair of MBSs. Thus, the other constituent MBS basically remains "invisible" to the tunneling lead. For instance, in Fig. 1(i), the tunnel lead, which couples from the left end, should couple much more strongly to only one of the MBSs (shown in blue), while coupling to the other MBS (shown in yellow) is strongly suppressed because of partial decoupling of the MBSs. Thus, the local coupling to a ps-ABS is effectively equivalent to the local coupling to a MZM.

In a recent preprint [50] it has been argued (based on a smooth confinement potential scenario similar to that proposed in Ref. [35]) that quantized conductance plateaus can also arise in the trivial regime due to differences in the spin polarization of the constituent MBSs, even if the MBSs are fully overlapping. By contrast, in this paper we find that for a steplike potential in the quantum-dot region, the stability of the quantized conductance plateaus is essentially controlled by the separation between the constituent MBSs of a ps-ABS, as shown in Fig. 2(p). The details of the relationship between the ps-ABSs found in this paper and the quasi-Majoranas emerging in the presence of a smooth confinement potential as described in Refs. [35,50], including the effects of spin polarizations and the spatial separation of the component MBSs on the stability of the conductance plateaus, will be addressed in a forthcoming publication. Based on the results of this paper, we conclude that the local charge tunneling measurement, which was, so far, the primary type of probe used in experiments, has exhausted its potential to reveal useful information regarding the distinction of MZMs from low-energy ABSs (ps-ABSs in particular), both of which can appear in SM-SC hybrid structures. The next stage must involve nonlocal probes, such as, for example, the two-terminal charge tunneling measurement [48,51].

ACKNOWLEDGMENTS

C.M., C.Z., and S.T. acknowledge support from ARO Grant No. W911NF-16-1-0182. T.D.S. was supported by NSF Grant No. DMR-1414683.

[1] J. D. Sau, R. M. Lutchyn, S. Tewari, and S. Das Sarma, Phys. Rev. Lett. **104**, 040502 (2010).

[2] S. Tewari, J. D. Sau, and S. D. Sarma, Ann. Phys. **325**, 219 (2010).

[3] J. Alicea, Phys. Rev. B **81**, 125318 (2010).
[4] J. D. Sau, S. Tewari, R. M. Lutchyn, T. D. Stanescu, and S. Das Sarma, Phys. Rev. B **82**, 214509 (2010).
[5] R. M. Lutchyn, J. D. Sau, and S. Das Sarma, Phys. Rev. Lett. **105**, 077001 (2010).
[6] Y. Oreg, G. Refael, and F. von Oppen, Phys. Rev. Lett. **105**, 177002 (2010).
[7] T. D. Stanescu, R. M. Lutchyn, and S. Das Sarma, Phys. Rev. B **84**, 144522 (2011).
[8] N. Read and D. Green, Phys. Rev. B **61**, 10267 (2000).
[9] A. Y. Kitaev, Phys. Usp. **44**, 131 (2001).
[10] C. Nayak, S. H. Simon, A. Stern, M. Freedman, and S. Das Sarma, Rev. Mod. Phys. **80**, 1083 (2008).
[11] C. Beenakker, Annu. Rev. Condens. Matter Phys. **4**, 113 (2013).
[12] S. R. Elliott and M. Franz, Rev. Mod. Phys. **87**, 137 (2015).
[13] V. Mourik, K. Zuo, S. M. Frolov, S. Plissard, E. P. Bakkers, and L. P. Kouwenhoven, Science **336**, 1003 (2012).
[14] M. Deng, C. Yu, G. Huang, M. Larsson, P. Caroff, and H. Xu, Nano Lett. **12**, 6414 (2012).
[15] A. Das, Y. Ronen, Y. Most, Y. Oreg, M. Heiblum, and H. Shtrikman, Nat. Phys. **8**, 887 (2012).
[16] L. P. Rokhinson, X. Liu, and J. K. Furdyna, Nat. Phys. **8**, 795 (2012).
[17] H. O. H. Churchill, V. Fatemi, K. Grove-Rasmussen, M. T. Deng, P. Caroff, H. Q. Xu, and C. M. Marcus, Phys. Rev. B **87**, 241401 (2013).
[18] A. D. K. Finck, D. J. Van Harlingen, P. K. Mohseni, K. Jung, and X. Li, Phys. Rev. Lett. **110**, 126406 (2013).
[19] S. M. Albrecht, A. Higginbotham, M. Madsen, F. Kuemmeth, T. S. Jespersen, J. Nygård, P. Krogstrup, and C. Marcus, Nature (London) **531**, 206 (2016).
[20] M. Deng, S. Vaitiekėnas, E. B. Hansen, J. Danon, M. Leijnse, K. Flensberg, J. Nygård, P. Krogstrup, and C. M. Marcus, Science **354**, 1557 (2016).
[21] H. Zhang, Ö. Gül, S. Conesa-Boj, M. P. Nowak, M. Wimmer, K. Zuo, V. Mourik, F. K. de Vries, J. van Veen, M. W. de Moor, J. D. S. Bommer, D. J. van Woerkom, D. Car, S. R. Plissard, E. P. Bakkers, M. Quintero-Pérez, M. C. Cassidy, S. Koelling, S. Goswami, K. Watanabe, T. Taniguchi, and L. P. Kouwenhoven, Nat. Commun. **8**, 16025 (2017).
[22] J. Chen, P. Yu, J. Stenger, M. Hocevar, D. Car, S. R. Plissard, E. P. Bakkers, T. D. Stanescu, and S. M. Frolov, Sci. Adv. **3**, e1701476 (2017).
[23] F. Nichele, A. C. C. Drachmann, A. M. Whiticar, E. C. T. O'Farrell, H. J. Suominen, A. Fornieri, T. Wang, G. C. Gardner, C. Thomas, A. T. Hatke, P. Krogstrup, M. J. Manfra, K. Flensberg, and C. M. Marcus, Phys. Rev. Lett. **119**, 136803 (2017).
[24] H. Zhang, C.-X. Liu, S. Gazibegovic, D. Xu, J. A. Logan, G. Wang, N. van Loo, J. D. Bommer, M. W. de Moor, D. Car, R. L. M. Op het Veld, P. J. van Veldhoven, S. Koelling, M. A. Verheijen, M. Pendharkar, D. J. Pennachio, B. Shojaei, J. S. Lee, C. J. Palmstrøm, E. P. A. M. Bakkers, S. Das Sarma, and L. P. Kouwenhoven, Nature (London) **556**, 74 (2018).
[25] K. Sengupta, I. Žutić, H.-J. Kwon, V. M. Yakovenko, and S. Das Sarma, Phys. Rev. B **63**, 144531 (2001).
[26] A. R. Akhmerov, J. Nilsson, and C. W. J. Beenakker, Phys. Rev. Lett. **102**, 216404 (2009).
[27] K. T. Law, P. A. Lee, and T. K. Ng, Phys. Rev. Lett. **103**, 237001 (2009).
[28] K. Flensberg, Phys. Rev. B **82**, 180516 (2010).
[29] D. Bagrets and A. Altland, Phys. Rev. Lett. **109**, 227005 (2012).
[30] J. Liu, A. C. Potter, K. T. Law, and P. A. Lee, Phys. Rev. Lett. **109**, 267002 (2012).
[31] W. DeGottardi, D. Sen, and S. Vishveshwara, Phys. Rev. Lett. **110**, 146404 (2013).
[32] W. DeGottardi, M. Thakurathi, S. Vishveshwara, and D. Sen, Phys. Rev. B **88**, 165111 (2013).
[33] D. Rainis, L. Trifunovic, J. Klinovaja, and D. Loss, Phys. Rev. B **87**, 024515 (2013).
[34] İ. Adagideli, M. Wimmer, and A. Teker, Phys. Rev. B **89**, 144506 (2014).
[35] G. Kells, D. Meidan, and P. W. Brouwer, Phys. Rev. B **86**, 100503 (2012).
[36] D. Chevallier, D. Sticlet, P. Simon, and C. Bena, Phys. Rev. B **85**, 235307 (2012).
[37] D. Roy, N. Bondyopadhaya, and S. Tewari, Phys. Rev. B **88**, 020502 (2013).
[38] P. San-Jose, J. Cayao, E. Prada, and R. Aguado, New J. Phys. **15**, 075019 (2013).
[39] T. Ojanen, Phys. Rev. B **87**, 100506 (2013).
[40] T. D. Stanescu and S. Tewari, Phys. Rev. B **89**, 220507 (2014).
[41] J. Cayao, E. Prada, P. San-Jose, and R. Aguado, Phys. Rev. B **91**, 024514 (2015).
[42] J. Klinovaja and D. Loss, Eur. Phys. J. B **88**, 62 (2015).
[43] P. San-Jose, J. Cayao, E. Prada, and R. Aguado, Sci. Rep. **6**, 21427 (2016).
[44] C. Fleckenstein, F. Domínguez, N. Traverso Ziani, and B. Trauzettel, Phys. Rev. B **97**, 155425 (2018).
[45] D. I. Pikulin, J. Dahlhaus, M. Wimmer, H. Schomerus, and C. Beenakker, New J. Phys. **14**, 125011 (2012).
[46] E. Prada, P. San-Jose, and R. Aguado, Phys. Rev. B **86**, 180503 (2012).
[47] C.-X. Liu, J. D. Sau, T. D. Stanescu, and S. Das Sarma, Phys. Rev. B **96**, 075161 (2017).
[48] C. Moore, T. D. Stanescu, and S. Tewari, Phys. Rev. B **97**, 165302 (2018).
[49] C. W. Groth, M. Wimmer, A. R. Akhmerov, and X. Waintal, New J. Phys. **16**, 063065 (2014).
[50] A. Vuik, B. Nijholt, A. Akhmerov, and M. Wimmer, arXiv:1806.02801 (unpublished).
[51] S. Das Sarma, J. D. Sau, and T. D. Stanescu, Phys. Rev. B **86**, 220506 (2012).